RSC Advances

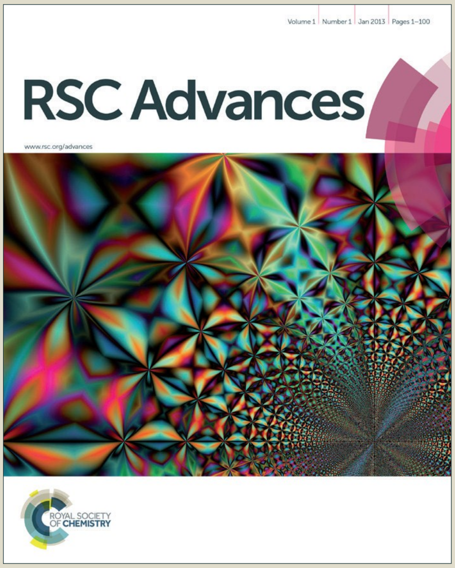

Synthesis of bentonite clay based hydroxyapatite nanocomposite cross-linked by glutaraldehyde and optimization by response surface methodology for lead removal from aqueous solution

Piyali Roy Choudhury[1], Priyanka Mondal[1], Swachchha Majumdar[1]*

[1]Ceramic Membrane Division, CSIR-Central Glass and Ceramic Research Institute, 196, Raja S. C. Mullick Road, Kolkata- 700 032, India

*Corresponding author address:
S. Majumdar
Email: swachchha@cgcri.res.in
Tel. +91 33 2473 3252
fax: +91 33 2473 0957

Abstract

A novel nanocomposite (BT-HAp) was developed by chemical synthesis of hydroxyapatite nanoparticles and bentonite clay that further applied for toxic lead (Pb) removal from aqueous solution. Three types of bentonite clay based nanocomposite were prepared by varying the pH of the solution (3, 7 and 10) and addition of glutaraldehyde as a cross-linking agent. The formation and performance of the prepared BT-HAps were examined herein. A clear and sharp XRD peaks suggested the presence of hydroxyapatite and bentonite clay compound in composite. FTIR spectrum confirmed the existence of functional groups required to develop the nanocomposite. The Bt-HAp nanocomposites were also characterized in terms of the BET, FESEM and TEM etc. to establish its formation. The synthesized nanocomposite showed highest sorption capacity at pH 7 than 3 and 10. A mathematical and statistical optimizing technique (response surface methodology) was applied to verify the interactive effects of various parameters on sorption capacity. The analysis of variance was discussed for factors and response, that confirmed the significance of the predicted model ($R^2 = 0.9906$). Langmuir isotherm model best represented the phenomenon having sorption capacity of 346 mg g^{-1} at 30° C. The sorption mechanism was well described by the Pseudo 2^{nd} order kinetic model indicating coexistence of both physisorption and chemisorption. Moreover, a considerable amount of toxic Pb (~99 %) removal was observed by the synthesized nanocomposite *via* sorption.

***Key Words**: Synthesis, Nanocomposite, lead removal, optimization.*

1. Introduction

Application of nanoparticles for contaminated water treatment has gained remarkable interest to the scientific community in recent time. The metal oxide nanoparticles like Al_2O_3, MnO_2, MgO and TiO_2 were used for heavy metal removal from aqueous system.[1] Similarly, silver nanoparticles also gained considerable attention for their antimicrobial activity.[2] Simeonidis et al. (2015) found that Fe magnetite nanoparticles (20 nm) were able to remove toxic chromium from drinking water.[3] The removal capacity of Cr by magnetic nanoparticle was 1.8 μg Cr (VI) $mg^{-1}$for a residual concentration of 50 μg l^{-1} at a neutral pH.[3] However, these nanoparticles have some disadvantages in terms of separation period and reusability of nanoparticles from treated water.[4-7] Therefore, it is utmost important to overcome these drawbacks to produce fresh water. The composite material has gained considerable research attention in recent years for toxic contaminants removal from aqueous system. These materials are easily separable from filtered water due to their comparatively large size. Nanocomposite consist two or more component having at least one in nano dimension with different chemical and physical properties than individual. However, development of nanocomposite in combination with nanoparticles (NPs) having superior property e.g. large surface area, surface reactivity and high mechanical stimuli can be a possible solution.[8, 9]

A significant threat occurs to the environment and public health due to the discharge of heavy metals especially Pb from printing, textile industries or other sources to the water body.[10] It can cause structural damage in the mammalian eye, central nervous system and blood cells.[11] Adsorption is widely used method for heavy metal remediation due to its simple and economic operation process compared to other conventional methods. In this context, the Pb adsorption by nanocomposite could be a feasible way to remediate toxic elements from aqueous solution.[12-17]

Natural and synthetic nanomaterials incorporated into other functional groups for getting the desired nanocomposite with significant performance has gained attention nowadays. Several clay based nanocomposites mixed with nanoparticles are reported for the removal of water contaminants. Chao et al. (2015) reported that the adsorption characteristics are strongly influenced by bentonite clay and metal oxide nanocomposite.[18] A new nanocomposite was developed by acid activated clay to study the adsorption feasibility of crystal violet dye.[19] Bentonite clay composite materials are now widely applied due to improved sorption time, efficiency and life cycles in water purification system including heavy metal adsorption, rather than insitu application.[19, 20-23] Bentonite clay based hydroxyapatite nanocomposite has not been reported till now. Although Cynthia et al. (2014) suggested that hydroxyapatite may be an alternative approach for removal of toxic contaminants.[24] Very recently, the synthesized hydroxyapatite have been combined with metal oxide nanoparticles for potential applications in water purification.[25-27]

It is well known that bentonite is a natural, low cost clay mineral and largely available material. Therefore, in this study a new nanocomposite was developed combining bentonite with hydroxyapatite nanomaterial (BT-HAp). Inclusions of ceramic material such as bentonite clay improve the sorption capacity as well as the mechanical properties of hydroxyapatite. Glutaraldehyde is used as a cross-linking agent to adhere the components in composite. Additionally, it has disinfectant property with low toxicity and also enhances the mechanical property of the nanocomposite.[28] Reports are not available to the best of our knowledge regarding bentonite clay based hyroxyapatite nanocomposite synthesis and its application as a sorbent for Pb removal from synthetic water.

Additionaly, effect of different independent variables on Pb sorption capacity has been optimized in this study. Central Composite Design (CCD) is considered to design the experimental data in Response surface methodology (RSM) optimization method. Moreover, the relationship of the response and the independent variable as pH, initial Pb concentration, dosage is established by statistical analysis.

2. Experimental

2.1. Materials

Calcium nitrate tetrahydrate ($Ca(NO_3)_2.4H_2O$) (99%); diammonium hydrogen phosphate ($(NH_4)_2HPO_4$), (99%); ammonia ($NH_3.H_2O$); glutaraldehyde; lead nitrate ($Pb(NO_3)_2$) (99%); from Merck, Germany were used. Bentonite clay was obtained from CSIR-CGCRI, Kolkata, used without further purification.

2.2. Synthesis of hydroxyapatite NPs

The HAp nanoparticle synthesis was conducted by chemical precipitation method with some modification.[29] In brief, according to Ca/P ratio of 1.6:1, the Ca $(NO_3)_2$ and $(NH_4)_2HPO_4$ was dissolved in 100 ml Mili-Q water separately. The aqueous NH_3 was used to maintain the pH of the solutions at 10. The solution of Ca $(NO_3)_2$ was added dropwise into $(NH_4)_2HPO_4$ solution in rapid stirring (250 rpm) condition. Gelatin was added later as an adhesion material during the precipitation. The greenish precipitate was repeatedly washed to remove the impurities like ammonia and its by-products. Subsequently, the green compact was washed with Mili-Q water for several times. The solid product was oven dried at 50 ºC for overnight and sintered at 1200 ºC for 2 hrs. Finally, the calcined HAp was powdered for advance applications.

2.3. Preparation of BT-HAp nanocomposite

The equal ratio (1:1) of bentonite clay and synthesized hydroxyapatite NP was maintained for nanocomposite preparation. Both of the solutions (50 ml) were stirred (250 rpm) in a 250 ml beaker separately for 12 hrs. Hydroxyapaptite solution was then poured into the bentonite clay solution in continuous stirring condition. Glutaraldehyde (6ml to 100ml) was added drop wise to the solution mixture as a crosslinker. Three sets of experiments were conducted at different pH range such as 3, 7 and 10. The pH was adjusted by using of 0.1 (N) HCl and 0.1 (N) NaOH solutions. Finally all the solutions were stirred at 250 rpm for 12 hrs at room temperature. Washing-centrifugation procedure was then followed to make the neutral supernatant. Finally, prepared BT-HAp nanocomposite was dried at 60 °C for 2 hrs and powdered by mortar pestle. Fig. 1 shows the schematic of the nanocomposite formation process with changes of morphology. The prepared samples were stored in the air tight container for further uses.

2.4. Experimental design

RSM is a well known optimization approach that simultaneously considers several parameters at different design levels. Moreover, this mathematical and statistical modeling tool is used to achieve the desired product with less number of experiments without the requirement of observing all probable combinations experimentally.[30-34] Central composite design was undertaken to establish the relationship between the independent variables with the response of the Pb sorption capacity. Two-level three factors (2^3) were employed with a series of experiments. Design Expert software was also used to express the regression model and graphical analysis of the data. Coded level (-1,0,+1) of variables *viz.*, nanocomposite dosage 0.5-1.5 g L^{-1} (A), initial Pb concentration 50-150 (B) mg L^{-1} and initial solution pH 4.1-6.1(C) were designed by CCD to study the effects on sorption capacity (Table 1).

The quadratic model was designed by CCD and the response variables were expressed as a function of process variables. In this method, a set of twenty experiments were conducted. The quadratic model for optimum value calculation is represented below

$$Y = \beta_0 + \sum_{i=1}^{k} \beta_i x_i + \sum_{i=1}^{k} \beta_{ii} x_i^2 + \sum\nolimits_{i=1} \sum_{j=i+1} \beta_{ij} x_i x_j \qquad (1)$$

where, β_0 is constant, β_i, β_{ii}, β_{ij} are regression coefficients and x_i, x_j denotes the independent variables. Predicted response is represented as Y.[35]

In this study, the independent given variables were considered as pH, initial Pb concentration and nanocomposite dosage, whereas sorption capacity was dependent experimental response.

2.5. Material characterization

The X-Ray Diffraction (XRD) analysis of the BT-HAp nanocomposite was performed by Philips 1710 diffractometer using Cu as anode (Netherlands). The morphology of the powdered sample was investigated using field emission scanning electron microscopy (FESEM, Gemini Zeiss Supra^{TM}, 35 VP Model, Germany). Moreover the qualitative energy dispersive X-ray spectroscopy (EDX, Leo S430I, U.K and Carl Zeiss, ΣIGMA-Germany) was used to detect the elements presents in samples. Various functional groups were detected by Fourier transform infrared spectroscopy (FTIR, Perkin Elmer, USA). The surface area was measured by adsorption-desorption of nitrogen using multipoint Braunauer-Emmett-Teller (BET) method by using Quantachrome (USA). Transmission electron micrograph (TEM, Technai G2 30ST-FEI, USA), particle size distribution of synthesized materials (Zetasizer, Nanoseries, Malvern) were also used to understand the nature of the synthesized powder. The solution pH was measured by pH meter (EUTECH, India). After adsorption processes, Pb contaminated nanocomposite was also characterized for any changes of functional groups or morphology.

2.6. Lead adsorption experiments

The adsorption study was carried out in batch mode. All solutions were prepared using ultrapure water from Milipore-Q (USA) system. The synthetic solutions at different concentrations were prepared by diluting the standard Pb solution (1000 mg L^{-1}) obtained by dissolving quantitatively $Pb(NO_3)_2$ in Mili-Q water at room temperature. The sample of 10 ml volume was collected at different initial concentration with nanocomposite dose of 1 g L^{-1}. Adsorption studies were performed in a batch reactor at 250 rpm by magnetic stirrer for 24 h. The pH, nanocomposite dosage, initial Pb concentration variations were conducted for efficient Pb sorption studies. In addition, the Pb sorption was carried out at different temperature to observe its effect on removal efficiency. The concentration of Pb was measured by ion chromatography (881 Compact IC pro, Metrohm). The repeatability study was carried out for all experiments and the errors were found minimum. The sorption capacity q_e (mg g^{-1}) and removal efficiency (R) were calculated from the following equations:

$$q_e = V\left(C_0 - C_e\right)/m \qquad (2)$$

$$R = \left(C_0 - C_e\right)/C_0 \times 100 \qquad (3)$$

where, V is the volume of solution (L), C_0 & C_e are the initial and equilibrium Pb concentration (mg L^{-1}), m (g) is the mass of the nanocomposite as adsorbent.

2.7. Desorption study

Desorption study was accomplished in batch mode with 0.1 M Ethylene diamine tetra acetic acid (EDTA), NaOH and HNO_3. The other conditions remained unchanged and about 0.01 g spent nanocomposite were taken for each solution. Desorption study was carried out at 250 rpm for 180 minutes at 30° C. Desorption efficiency was estimated from the following standard equation:

$$\%Desorption = C_d / C_a \times 100 \qquad (4)$$

where, C_d and C_a are the amount of metal ion desorbed and adsorbed in mg L^{-1}.

3. Results and Discussion

3.1. Characterization of nanocomposite

The XRD patterns of BT-HAp nanocomposite are shown in Fig. 2(a-c). The crystal phase was obtained by XRD analysis clearly shows the increase in crystalinity for BT-HAp nanocomposite at pH 7 (Fig. 2b) than BT-HAp at pH 3 and 10 (Fig. 1a and 1c). This result demonstrated about high crystalline structure of BT-HAp-7. The sharp and major peaks related to HAp were observed as 25.94, 29.02, 31.89, 32.28, 33.0, 34.15, 39.93, 49.6, 53.3 at 2θ degree. The positions and d-values were well matched with JCPDS No. 09-0432.[26] However, the peaks at 2θ = 5.3, 24.5, 34.7, 63.2 confirmed the presence of bentonite clay in composite. The similar findings were reported previously by T. S. Anirudhan et al, 2006.[36] Therefore, the formation of nanocomposite by BT-HAp was justified by XRD analysis. The crystallite size was estimated by Scherrer's equation from XRD pattern, $D = \kappa\lambda / \beta \cos\theta$, where constant k is 0.9-1, λ is the X-ray wavelength, β is the full width half maxima and θ is the Bragg's angle. The crystallite sizes of BT-HAp-3, 7, 10 were 28.6 nm, 36.7 nm and 45.9 nm, respectively.

In Fig. 3, FTIR spectra a, b and c denotes the synthesized nanocomposite BT-HAp-3, 7, and 10. The functional groups of the composite material were present in above mentioned three type of nanocomposite with variation of transmittance. The absorption bands at 3627-3630 cm^{-1} were assigned to the hydroxyl group (-OH). The broad absorption bands at 3434 and 1633 cm^{-1} may be attributed to the –OH stretching and bending, respectively for absorption of water molecules on clay and hydroxyapatite surface. Chemical cross-linker glutaraldehyde helped to attach the active groups (e.g. aldehyde) of HAp particle or clay mineral with each other.[37] Absorption bands at 1040-1044 cm^{-1} signifies the presence of Si-O-Si bond in BT-HAp. Additionally, another form of silica was observed at 522-527 cm^{-1}, respectively for the BT -HAp nanocomposite prepared at pH 3, 7 and 10. The presence of typical vibrations of 6 member rings compiled with alumina and silica-oxygen tetrahedral at 633 cm^{-1}.[38] The –PO$_4$ characteristic groups were assigned to the absorption band at 1036-1043 cm^{-1} which confirms the presence of hydroxyapatite in BT-HAp nanocomposite. In addition, the occurrence of hydroxyapatite in nanocomposite may be verified by the absorption band in FTIR spectra. Thus, above observation clearly indicates the formation of BT-HAp nanocomposite. After sorption of Pb, the intensity was shifted and the reduced intensity of OH^{-1} group is shown in Fig. 3 (d). The change in the FTIR spectrum after Pb sorption clearly demonstrated that the Pb ions were adsorbed on BT-HAp surface due to electrostatic attraction which signifies the physical sorption process.[39] The FESEM images (Fig. 4 (a-e)) describes surface morphology of the synthesized powder before and after sorption process. Fig. 4(a) signifies about the formation of nearly uniform spherical HAp nanoparticles with the particle size of 35-40 nm. The EDX analysis associated with FESEM was very useful to detect the elemental composition of the nanocomposite. The EDX analysis (inset of Fig. 4a) confirmed the presence of calcium, phosphate and oxygen elements in HAp nanoparticle. On the other hand, from Fig. 4(b-d) the porous surface of nanocomposite and the particle size varied from 75-80 nm was observed. In Fig. 4(e), the micrograph revealed Pb sorption on the nanocomposite surface that was also confirmed by EDX analysis (inset of fig. 4e).

The bright field TEM image confirmed the nanocomposite size ranges from 50-80 nm with porous surface (Fig. 5(a-c)). The HRTEM images are presented in the inset of TEM images of the particular nanocomposite. The interlayer spacing is equal to 0.294 nm of BT-HAp-7 nanocomposite in the HRTEM corresponds to the (211) plane. From low resolution of TEM image, the characteristic crystalline spot were obtained from SAED pattern (Fig. 5 d-f). The diffraction rings and bright spots were due to polycrystalline nature of the nanocomposite. A very clear rings and spots of nanoparticles suggested about the formation of highly crystalline BT-HAp-7 (Fig. 5e). Similar observation was also found in XRD pattern.

The surface area was measured by absorption-desorption of nitrogen by multipoint BET method. Further chemical treatment was not performed. The samples were under degassing at a temperature of 200 ºC for 2 hrs followed by flushing by helium gas. The moisture content and unwanted air was removed from the pores of the samples by helium degassing. The relative pressure was maintained in the range of 0.05-0.3 to measure the surface area. The surface area of BT-Hap was decreased as the pH of solution increases (pH 3- 21.89, pH 7- 12.4, pH 10- 11.9 m^2 g^{-1}) and therefore, the maximum surface area was obtained for BT-HAp-3. However, the particle size of the nanocomposite behaves inversely with the surface area and it increased with increasing solution pH. The crystallite size is also observed earlier in the same pattern. The average pore diameter and pore volume was determined by Barret-Joymer-Halender (BJH) method. It was observed that the pore diameter and pore volume were much higher (e.g. HAp-7: 522.9Å and 0.1627 cc g^{-1}) which plays a significant role for sorption of metal ions. From intensity vs. particle diameters plot, it was observed that the average particle size (d_{50}) of the nanoparticle was obtained around 100 nm.

3.2. Response surface optimization: ANOVA result

According to the design matrix by CCD, ANOVA results from software are listed in Table 3. A quadratic regression model equation describing the sorption process resulted from ANOVA study can be expressed as follows:

$$\begin{aligned} \mathit{Sorption\ Capacity} &= +97.72 + 1.29A - 13.87B + 0.48C - 1.04A^2 - 11.23B^2 - 1.2C^2 \\ &\quad + 0.074AB - 1.51AC - 0.14BC \end{aligned} \qquad (5)$$

The above regression model shows the relation between the response and the independent variable in terms of coded factor. It can be predicted from the equation that the dosage and solution pH has a positive effect on adsorption and initial Pb^{+2} concentrations have negative effect on sorption capacity. The highest order of the significant effect by different independent variable and their interactions on sorption capacity is B and lowest is AB. ANOVA study was performed to justify the significance of the quadratic model. The model F-value of 117.34 implies the significance of the model (Table 3). There was only 0.01% possibility to make noise in the predicted model. A good correlation was observed between the experimental data and predicted data. The multiple correlation coefficient (R^2) was found as 0.9906 which implies that 99.06% of the variations of sorption capacity could be explained by the model. The ‘Pred R^{2}’ of 0.9051 was in logical conformity with the ‘Adj R^{2}’ of 0.9822.

3.3. Interactive effect of variables on sorption capacity

The effect of experimental variables and the response of sorption capacity were analyzed which was designed by CCD with full factorial based on three factors. Table 4 represents a comparative study on Pb sorption capacity among the nanocomposites and its basic components with 100 mg L^{-1} initial Pb solution at pH 7. The maximum sorption capacity was found for BT-HAp-7 nanocomposite (97.94 mg g^{-1}) than BT-HAp-3 (95 mg g^{-1}) and 10 (93 mg g^{-1}) which are shown in table 4. Hence, all the sorption experiments were carried out by potential BT-HAp-7 nanocomposite. Although bentonite clay (78 mg g^{-1}) and HAp nanoparticles (83 mg g-^{1}) individually did not show good sorption capacity compared to BT-HAp nanocomposite, combination of these two components were explored for potential capacity. It was reported that particle sizes influenced the sorption process noticeably during in situ application of nanoparticles.[43] Results shows that although BT-HAp-7 nanocomposite has less surface area than BT-HAp-3, it has got better adsorption property than BT-HAp-3. Therefore, particle size was not solely responsible for sorption capacity. The Pb solution was possibly able to diffuse through the particles and a poor correlation might obtain by external surface, suggests that particle size was not the prime parameter to control the equilibrium sorption. However, at equilibrium, the sorption capacity and specific surface area were not directly proportional to each other. [17] Fig. 6(a) reveals the combine effect of dose corresponding with initial Pb concentrations on sorption capacity of nanocomposite in contour plot. In this plot, we observed that the sorption capacity was increases with increasing dosage whereas at the same time under same experimental condition, sorption capacity was decreased with increasing Pb concentration. The sorption capacity was reduced from 99.4 % to 75% with increasing Pb concentration from 50 mg L^{-1} to 150 mg L^{-1} with 1 mg L^{-1} dose, therefore, metal ion uptake by the nanocomposite was reduced by decreasing driving force in form of concentration gradient. On other hand the sorption capacity was enhanced with increasing dosage of nanocomposite due to attachment of Pb with the higher surface area of nanocomposite.

The combine effect of dose and the solution pH on Pb removal are shown in Fig. 6(b). It was observed that the sorption capacity was increases with increasing nanocomposite dosage. It was also found by quadratic model that the dose parameter have positive effect on sorption capacity however, change in sorption capacity beyond 1 g L^{-1} dose considering 100 mg L^{-1} Pb^{+2} concentration was insignificant. Therefore, the optimum dose was considered as 1 g L^{-1} with same experimental condition. The solution pH is an important factor that significantly influenced the sorption capacity or removal efficiency. The contour plot revealed that the sorption capacity was increases from 96% to 99.4% with increasing pH from 4.5 to 5, respectively. However, the sorption capacity was decreases from 99.48 to 97.8% with changing pH from pH 5 to 5.5, respectively. At a lower pH (<5), BT-HAp nanocomposite surfaces become positively charged due to higher H^+ ion concentration, resulting lower sorption capacity due to repulsion between positively charged nanocomposite surface and Pb^{+2}. The solution was favored higher sorption capacity at pH 5 due to electrostatic attraction between negatively charged BT-HAp nanocomposite surface and the Pb^{+2}. Although beyond this pH, the sorption experiment was unsuccessful due to precipitation of Pb as lead hydroxide.[41] Hence, selection of exact pH is very important and in this study optimum pH was found as 5 by response surface methodology.

The pH has a positive effect on sorption capacity (Eqn. 5). Fig. 6(c) represents the collective effect of pH and initial Pb concentration on sorption capacity. The sorption capacity was decreases from 99.4% to 75% with increasing Pb concentration from 50 to 150 mg L^{-1} by applying 1 g L^{-1} dose at pH 5. The nanocomposite active sites were enclosed by more Pb ions and get saturated when higher Pb concentration was used and therefore, sorption capacity decreases.[42] Similar observations were also found for other pH values.

3.4. Validation and confirmation of model

Validation is a technique of RSM that used to check the accuracy of the predicted model and the corresponding results are shown in Table 2. Assessment of experimental test and predicted findings confirms similar responses (Fig 7). The software was allowed to select the targeted goal for factors or responses from numerical optimization. In this study, the factors were within the range and based on corresponding 10 optimum conditions, the sorption capacities was about 97.94 mg g^{-1} with 0.95% deviation from experimental value. From 10 optimum conditions in numerical optimization method, the desirability as an objective function was found out 1 by considering the desired goals (Table 5). Therefore, the regression model successfully explained the process with high accuracy and reliable for predicting the sorption capacity.[32]

3.5. Adsorption isotherm and kinetics

Sorption capacity estimation is necessary to ascertain the amount of sorbent required for potential removal of heavy metal such as Pb from aqueous solution. Adsorption isotherm study was conducted by varying the Pb concentration from 50 to 150 mg L^{-1} with dosage of 1 g L^{-1} for 24 hrs contact time. Temperature was varied as 20º, 30º and 50º C to conduct the isotherm study.

Equilibrium data was further analyzed by Langmuir and Freundlich isotherm model to understand the sorption behavior. The Langmuir model is based on monolayer coverage with homogeneous surface sites whereas Freundlich model is applicable only for highly heterogeneous surfaces.[43, 44] Table 6 represents the result of isotherm model and we observed that Langmuir model fitted well with co-relation coefficient (R^2) of 0.99. The higher n value indicates the favorable condition of adsorbate on sorbent surface. Pb monolayer was bonded with functional groups of BT-HAp-7 nanocomposite during sorption. The maximum sorption capacity was found as 346 mg g^{-1} that was significantly higher compared to other materials shown in the table 7.

Pseudo kinetic models were studied to observe the sorption mechanism. The Pseudo 1st order and 2nd order kinetic models with the empirical equations were used to determine the rate kinetics.[49] It was observed that the sorption capacity was very fast within first 15 minutes but after that the process became slower before reaching equilibrium. The pseudo 2nd order model was best fitted with linear regression correlation coefficient (R^2) value of 0.999. The rate constant (k_2) value indicated the chemisorptions process of Pb ions on the nanocomposite surface.[50]

3.6. Desorption study of nanocomposite

The adsorbents were loaded with toxic heavy metals which results an environmental hazard solid spent waste. Therefore, regeneration of spent materials can make the process cost-effective. Desorption study was conducted using EDTA, HNO_3 and NaOH solution. Maximum desorption about 64% from spent nanocomposites containing 97 mg g^{-1} of Pb was observed using EDTA solution whereas only 0.12% for and 0.01% desorption was observed for HNO_3 and NaOH, respectively at 60 minutes contact time. Equilibrium was reached after 120 minutes at constant stirring condition. Three consecutive sorption-desorption cycles were performed and sorption capacity of the nanocomposite decreases about 12-16% during this period. Y. Ren et al.(2012) discussed that the sorption-desorption process involved the complexation, physisorption and ion exchange reaction.[50] However, the reason behind improved desorption efficiency of EDTA solutions can be explained by the reaction of loosely bound Pb^{+2} with EDTA, that produced a stable lead acetate complex and desorbed quickly. Therefore, nanocomposites were regenerated for further uses.[51]

4. Conclusions

The nanocomposite (BT-HAp) was successfully synthesized from bentonite clay and hydroxyapatite by chemical synthesis method. The novelty of this work lies on development of three different nanocomposite from clay and HAp powder having distinguished property. Additionally, the novel nanocomposite was potentially applied for toxic heavy metal (Pb) remediation. A very simple synthesis process is discussed in this report, where raw materials are of very low-cost. Hence there is a possibility to scale-up the process in a cost-effective manner with a less hazardous component. BT-HAp nanocomposite was synthesized at neutral pH which is very significant for application in natural condition and use of minimum chemicals makes the process environment friendly. The formation of BT-HAp nanocomposite was confirmed through XRD, FTIR, FESEM, EDX and TEM analysis. BT-HAp-7 was established as potential sorbent having less surface area than BT-HAp-3. This observation indicated that the external surface was not the main parameter for sorption. The ANOVA results showed optimization of Pb sorption on nanocomposite by RSM was in well agreement with experimental result under optimized condition. The multiple correlation coefficient (R^2=0.9906) value was also justified the above observations. The model designed by CCD well describes the sorption process where the sorbent dose and the pH have a positive effect. However, initial Pb concentration had negative effect on sorption process. The Numerical optimization method showed that Pb sorption capacity of nanocomposite was about 97.94 mg g^{-1}. The sorption process fits well with the Langmuir isotherm model signifies monolayer Pb sorption on nanocomposite surface. The sorption mechanism of nanocomposite was also well explained by Pseudo 2nd order model indicated chemisorption. In summary, the experimental and theoretical results suggest that BT-HAp nanocomposite could be a potential, low cost sorbent for heavy metal remediation from waste water towards an environmental friendly approach.

Acknowledgement

This work was financially supported by Council of Scientific and Industrial Research, New Delhi, India.

References

1 K. Simeonidis, S. Mourdikoudis, E. Kaprara, M. Mitrakas and L. Polavarapu, *Environ. Sci.:Water Res. Technol.*, 2015, Advance Article.

2 L. Cui, P. Chen, S. chen, Z.Yuan, C.Yu, Bin Ren and K. Zhang, *Anal. Chem.*, 2013, 85, 5436.

3 K. Simeonidis, E. Kaprara, T. Samaras, M. Angelakeris, N. Pliatsikas, G. Vourlias, M. Mitrakas and N. Andritsos, Optimizing magnetic nanoparticles for drinking water technology: The case of Cr(VI), *Sci. Total Environ.*, 2015, 535, 61.

4 Y. L. F. Musico, C. M. Santos, M. L. P. Dalidab and D. F. Rodriguesa, Improved removal of lead (II) from water using a polymer-based graphene oxide nanocomposite, *J.Mater. Chem. A*, 2013, 1, 3789.

5 S. Pal, A. S. Patra, S. Ghorai, A.K. Sarkar, R. Das and S. Sarkar, Modified guar gum/SiO_2: development and application of a novel hydrid nanocomposite as a flocculant for the treatment of wastewater, *Environ. Sci.: Water Res. Technol.*, 2015, 1, 84.

6 A. Mahapatra, B.G. Mishra and G. Hotan, Adsorptive removal of Congo red dye from waste water by mixed iron oxide-alumina nanocomposite, *Ceram. Int.*, 2013, 39, 5443.

7 Y. Liu, c. Luo, J. Sun, H. Li, Z. Sun and S. Yan, Enhanced adsorption removal of methyl orange from aqueous solution by nanostructured proton- containing δ-MnO_2, *j. Mater. Chem. A*, 2015, 3, 5674.

8 K. Kalpana and V. Selvaraj, A novel approach for the synthesis of highly active $ZnO/TiO_2/Ag_2O$ nanocomposite and its photocatalytic applications, *Ceram. Int.*, 2015, 41, 9671.

9 Y. Lu, Y. Yang, A. Sellinger, M. Lu, J. Huang, H. Fan, R. Haddad, G. Lopez, A. R. Burns, D. Y. Sasaki, J. Shelnutt and C. J. Brinker, Self-assembly of mesoscopically ordered chromatic polydiacetylene/silica nanocomposites, *Nature*, 2001, 410, 913.

10 M. D. C. Hernández-Sariano, A. Pena and M. D. Mingorance, Environmental hazard of cadmium, copper, lead and zinc in metal-contaminated soils remediated by sulfosuccinamate formulation, *J. Environ. Monit*., 2011, 13, 2830.

11 A. B. G. Lansdown in Metal Ions Toxicology: Effects, Interactions, Interdependencies, *RSC*, 2011, vol. 8, ch. 9, 187.

12 S. S. Samandari, S. S. Samandari, N. Nezafati and K. Yahyaa, Efficient removal of lead(II) ions and methylene blue from aqueous solution using chitosan/Fe-hydroxyapatite nanocomposite beads, *J. Environ. Manage.*, 2014, 146, 481.

13 L. Aroui, L. Zerroual, M. Boutahalab, Synthesis and characterization of a PbO_2-clay nanocomposite: removal of lead from water using montmorillonite, *Mater. Res. Bull.*, 2012, 47, 206.

14 S. Ghorai, A. Sinhamahapatra, A. Sarkar, A. B. Panda and S. Pal, Novel biodegradable nanocomposite based on XG-g-PAM/SiO_2: application of an efficient adsorbent for Pb^{+2} ions from aqueous solutions, *Bioresour. Technol.*, 2012, 119, 181.

15 C. M. Futalan, C. C. Kan, M. L. Dalida, K. J. Hsien, C. Pascuad and M. W. Wan, Comparative and competitive adsorption of copper, lead and nickel using chitosan immobilized on bentonite, *Carbohydr. Polym.*, 2011, 83, 528.

16 N. P. J. Jovicic, A. D. M. Nikolic, M. J. Zunic, Z. D. Mojovic, P. T. Bankovic, I. A. Grzetic and D. M. Jovanovic, Synergic adsorption of Pb^{+2} and reactive dye-RB5 on two series of organomodified bentonites, *J. Contam. Hydrol.*, 2013, 150, 1.

17 R. Han, W. Zou, Z. Zhang, J. Shi and J. Yang, Removal of copper (II) and Pb (II) from aqueous solution by manganese oxide coated sand I. Characterization and kinetic study, *J. Hazard. Mater.*, 2006, 137, 384.

18 C. Yanga, Y. Zhua, J. Wanga, Z. Lia, X. Sua and C. Niub, Hydrothermal synthesis of TiO_2-WO_3-bentonite composites: conventional versus ultrasonic pretreatments and their adsorption of methylene blue, *Appl. Clay Sci.*, 2015, 105, 243.

19 A. A. Oladipo and M. Gazi, Enhanced removal of crystal violet by low cost alginate/acid activated bentonite composite beads: optimization and modeling using non-linear regression technique, *Journal of Water Process Engineering*, 2014, 2, 43.

20 E. I. Unuabonah and A. Taubert, Clay-polymer nanocomposites (CPNs): adsorbent of the future for water treatment, *Appl. Clay Sci.*,2014, 99, 83.

21 X. Wang, L.Yang, J.Zhang, C. Wang and Q. Li, Preparation and characterization of chitosan-poly(vinyl alcohol)/bentonite nanocomposite for adsorption of Hg(II) ions, *Chem. Eng. J.*, 2014, 251, 404.

22 M. E. Parolo, G. R. Pettinari, T. B. Musso, M. P.S. Izquierdo and L. G. Fernandez, Characterization of organo-modified bentonite sorbents: The effects of modification conditions on adsorption performance, *Appl. Clay Sci.*, 2014, 320, 356.

23 S. Sen gupta and K. G. Bhattacharyya, Adsorption of metal ions by clays and inorganic solids, *RSC. Adv.*, 2014, 4, 28537.

24 C. M. Kanno, R. L. Sanders, S. M. Flynn, G. Lessard and S. C. B. Myneni, Novel apatite-based sorbents for defluoridation: synthesis and sorption characteristics of nano-micro-crystalline hyroxiapatite-coated limestone, *Environ. Sci. Technol.*, 2014, 48, 5798.

25 W. Kantana, P. Jarupoom, K. Pengpat, S. Eitssayeam, T. Tunkasiri and G. Rujijanagul, Properties of hydroxiapatite/zirconium oxide nanocomposites, *Ceram. Int.*, 2013, 39, S379.

26 A. Farzadi, M. Solati-Hashjin, F. Bakhshi and A. Aminian, Synthesis and characterization of hydroxiapatite/b-tricalcium phosphate nanocomposites using microwave irradiation, *Ceram. Int.*, 2011, 37, 65.

27 H. EI. Khal and N. H. Batis, Effects of temperature on the preparation and characteristics of hydroxyapatite and its adsorptive properties toward lead, *New. J. Chem.*, 2015, 39, 3597.

28 Y. Q. Tan, Y. H. Song and Q. Zheng, Facile regulation of glutaraldehyde-modified graphene oxide for preparing free-standing papers and nanocomposite films. *Chin. J. Polym. Sci.*, 2013, 31, 399.

29 C. Shu, Y. Xianzhu, X. Zhangyin, X. Guohua, L. Hong and Y. Kangde, Synthesis and sintering of nanocrytalline hydroxyapatite powders by gelatin based precipitation method, *Ceram Int.*, 2007, 33, 193.

30 G. Wang, S. Zhang, T. Li, X. Xu, Q. Zhong, Y. Chen, O. Deng and Y. Li, Application of response surface methodology for optimization of lead removal from contaminated soil using chelants, *RSC Adv.*, 2015, 5, 58010.

31 H. Farnoush, J. A. Mohandesi, D. H. Fatmehsari and F. Moztarzadehb, A kinetic study on the electrophoretic deposition of the hydroxyapatite-titania nanocomposite based on a statistical approach, *Ceram Int.*, 2012, 38, 6753.

32 A. Witek-Krowiak, K. Chojnacka, D. Podstawczyk, A. Dawiec and K. Pokomeda, Application of response surface methodology and artificial neural networks method in modelling and optimization of biosorption process, *Bioresour. Technol.*, 2014, 160, 150.

33 K. Anupam, S. Dutta, C. Bhattacharjee and S. Datta, Adsorptive removal of chromium (VI) from aqueous solution over powder activated carbon: optimization through response surface methodology, *Chem. Eng. J.*, 2011, 173, 135.

34 K. Kalantari, M. B. Ahmad, H. R. F. Masoumi, K. Shameli, M. Basri and R. Khandanloum, Rapid and high capacity adsorption of heavy metals by Fe_3O_4 /montmorillonitrite nanocomposite using response surface methodology *J. Taiwan. Inst. Chem. E.*, 2014, doi: 10.1016/j.jtice.2014.10.025.

35 H. Chaair, J. C. Heughebaert, M. Heughebaert and M. Vaillant, Statistical analysis of apatitic tricalcium phosphate preparation, *J. Mater. Chem.*, 1994, 4, 765.

36 T. S. Anirudhan and M. Ramachandran, Adsorptive removal of tannin from aqueous solutions by cationic surfactant-modified bentonite clay, *J. Colloid Interface Sci.*, 2006, 299, 116.

37 B. Mohammed, D. Amina and G. Samira, The dicalcium phosphate dihydrate fixator and stabilizer of glutaraldehyde, *J. Mat. Sci. Eng. B Solid.*, 2013, 3, 605.

38 A. B. Đukić, K. R. Kumrić, N. S. Vukelić, Z. S. Stojanović, M. D. Stojmenović, S. S. Milošević and L. L. Matović, Influence of ageing of milled clay and its composite with TiO_2 on the heavy metal adsorption characteristics, *Ceram. Int.*, 2015, 41, 5129.

39 M. Danish, R. Hashim, M. Rafatullah, O. Sulaiman, A. Ahmad and Govind, Adsorption of lead (II) ions from aqueous solutions by date bead carbon activated with $Zncl_2$ *Clean-Soil, Air, Water*, 2011, 39, 392.

40 Y. Sag and Y. Aktay, Mass transfer and equilibrium studies for the sorption of chromium ions onto chitin, *Process Biochemistry*, 2000, 36, 157.

41 F. Ayari, E. Srasra and M. Trabelsi- Ayadi, Retension of lead from an aqueous solution by use of bentonite as adsorbent for reducing leaching from industrial effluents, *Desalination*, 2007, 206, 270.

42 P. Chand and Y. B. Pakade, Synthesis and characterization of hydroxyapatite nanoparticles impregnated on apple pomace to enhance adsorption of Pb(II), Cd(II) and Ni(II) ions from aqueous solution, *Environ. Sci. Pollut. Res.* 2015, 22, 10919.

43 C. H. Liu, Y. H. Chuang, T. Y. Chen, Y. Tian, H. Li, M. K. Wang and W. Zhang, Mechanism of arsenic adsorption on magnetite nanoparticles from water: Thermodynamic and spectroscopic studies, *Environ. Sci. Technol.*, 2015, 49, 7726.

44 J. Wang, G. Liu, T. Li and C. Zhou, Physicochemical studies toward the removal of Zn(II) and Pb(II) through adsorption on montmorillonite-supported zero-valent iron nanoparticles, *RSC Adv.*, 2015, 5, 29859.

45 M. S. Fernando, R. M. De Silva and K. M. N. De *Silva*, *Appl Surf. Sci*., 2015, 351, 95.

46 S. Saadat, A. K. Jashni and M. M. Doroodmand, *Journal of Environmental Chemical Engineering*, 2014, 2, 2059.

47 L. Yang, Z. Li, G. Nie, Z. Zhang and X. Lu, *Appl. Surf. Sci.*, 2014, 307, 601.

48 R. D. C. Soltani, G. S. Khorramabadi, A. R. Khataee and S. Jorfi, *J. Taiwan. Inst. Chem. E.*, 2014, 45, 973.

49 A. Dhillon and D. Kumar, Development of nanoporous adsorbent for the removal of health-hazardous fluoride ions from aqueous system, *J. Mater. Chem. A*, 2015, 3, 4215.

50 Y. Ren, N. Yan, J. Feng, J. Ma, Q. Wen, N. Li and Q. Dong, Adsorption mechanism of copper and lead ions onto grapheme nanosheet/ δ-MnO_2, *Materials Chemistry and Physics*, 2012, 136, 538.

51 L. Deng, Y. Su, H. Su, X. Wang and X. Zhu, Sorption and Desorption of lead (II) from wastewater by green algae *Cladophora fascicularis*, *J. Hazard. Mater.*, 2007, 143, 220-225.

List of Tables:

Table 1: Experimental range and levels (coded).

Table 2: 23 factorial design matrix and experimental response as sorption capacity (mg g^{-1}).

Table 3: ANOVA for the quadratic model.

Table 4: Comparative study of lead sorption capacity

Table 5: Numerical optimization of the experiment: 10 solutions with desirability of 1.

Table 6: Langmuir and Freundlich isotherm model parameters for lead sorption.

Table 7: Adsorption capacity of various nanocomposite.

List of Figures

Fig. 1: Schematic of nanocomposite process with changes in morphology.

Fig. 2: XRD pattern of nanocomposite for: BT-HAp- (a) pH-3, (b) pH-7 and (c) pH-10.

Fig. 3: FTIR spectra of the nanocomposite for: (a) pH-3, (b) pH-7,(c) pH-10, (d) after sorption, and (e) HAp Np.

Fig. 4: FESEM and EDX spectra: (a) HAp nanoparticles, nanocomposites: (b) BT-HAp-3, (c) BT-HAp-7, (d) BT-HAp-10 and (e) after sorption process.

Fig. 5: TEM image of BT-HAp nanocomposite: Bright field images (a-c) with HRTEM in inset and (d-f) SAED patterns.

Fig. 6: Contour plots demonstrating the influence of variables on sorption capacity. (a) dose vs. initial Pb conc., (b) dose vs. pH, (c) Initial Pb conc. vs pH.

Fig .7: Validity of model: Actual vs. predicted plot.

Tables

Table 1: Experimental range and levels (coded)

Independent variable	Factor code	Range and Level (Coded)		
		-1	0	+1
Dose, g L^{-1}	A	0.5	1	1.5
Initial Pb concentration, mg L^{-1}	B	50	100	150
pH	C	4.5	5	5.5

Table 2: 2^3 factorial design matrix and experimental response as sorption capacity (mg g^{-1})

Run	A: Dose	B: Initial Pb conc.	C: pH	Response: Sorption capacity, Actual value	Response: Sorption capacity, Predicted value
1	0.50	50.00	4.50	98	94.78
2	1.00	156.00	5.00	68	68.10
3	1.50	50.00	5.50	99	98.46
4	0.50	50.00	5.50	98.5	99.05
5	1.50	150.00	5.50	70	70.59
6	1.00	100.00	5.00	97	97.72
7	1.50	50.00	4.50	99	100.25
8	1.00	100.00	5.00	96.7	97.72
9	1.84	100.00	5.00	98.2	96.96
10	1.00	100.00	5.84	96	95.15
11	1.00	100.00	5.00	97.5	97.72
12	0.20	80.00	4.00	84	86.09
13	0.50	150.00	4.50	68	67.16
14	1.50	150.00	4.00	70	70.5
15	1.00	100.00	5.00	98	97.72
16	1.00	50.00	5.00	99	100.37
17	1.00	100.00	5.00	97.3	97.72
18	1.00	100.00	5.00	97.5	97.72
19	1.00	100.00	4.16	95.5	93.52
20	0.50	150.00	5.50	71	70.88

Table 3: ANOVA for the quadratic model

Source	Sum of squares	Degree of freedom (df)	Mean square	*F* -value	Probablity>F	Coefficient estimate
model	2973.11	9	330.35	117.34	<0.0001	-
A	17.08	1	17.08	6.07	0.0335	1.29
B	1911.58	1	1911.58	679.01	<0.0001	-13.87
C	3.61	1	3.61	1.28	0.2841	0.48
AB	0.041	1	0.041	0.015	0.9059	0.074
AC	30.09	1	30.09	10.69	0.0084	-1.51
BC	0.18	1	0.18	0.062	0.8082	-0.14
A^2	9.91	1	9.91	3.52	0.0900	-1.04
B^2	575.49	1	575.49	204.42	<0.0001	-11.23
C^2	30.77	1	30.77	10.93	0.0079	-1.20

$R^2 = 0.9906$, Adj $R^2 = 0.9822$, Pred $R^2 = 0.9051$

Table 4: Comparative study of lead sorption capacity.

Sorbent	Adsorption capacity, mg g^{-1}
BT-HAp-3	95
BT-HAp-7	97.94
BT-HAp-10	93
Bentonite clay powder	78
HAp nanopowder	83

Table 5: Numerical optimization of the experiment: 10 solutions with desirability of 1

A (Dose, g L^{-1})	B (Initial Pb concentration, mg L^{-1})	C (pH)	R1 (Sorption capacity, mg g^{-1})
0.80	97.33	5.13	97.9469
1.01	149.53	4.66	72.2151
0.65	99.96	4.74	95.1846
0.53	87.31	4.77	97.2562
0.76	100.15	4.83	96.2751
0.79	98.81	5.36	97.5142
0.69	128.46	5.15	85.2497
1.34	93.27	5.43	98.4342
1.10	111.00	5.50	93.3238
0.60	94.23	5.43	98.0828

Table 6: Langmuir and Freundlich isotherm model parameters for lead sorption

Langmuir model			Freundlich model		
R^2	q_m (mg g^{-1})	K_L (L mg^{-1})	R^2	K_F mg g^{-1}(mg L^{-1})^n	n
0.99	346	0.015	0.97	2.6	1.39

Table 7: Adsorption capacity of various nanocomposite

Nanocomposite	Adsorption capacity, mg/g	Reference
AC-HAp	9-14	M.S. Fernando et al.[45] doi:10.1016/j.apsusc.2015.05.092
SWCNTs/WSh	185.2	S.Saadat et al.[46] doi:10.1016/j.jece.2014.08.024
Poly(o-phenylenediamine) /reduced graphene oxide	228	L. Yang et al.[47] doi:10.1016/j.apsusc.2014.04.083
Silica nanopowders/alginate	83.33	R. D. C. Soltani et al.[48] doi:10.1016/j.jtice.2013.09.014
BT-HAp	**346**	**This study**

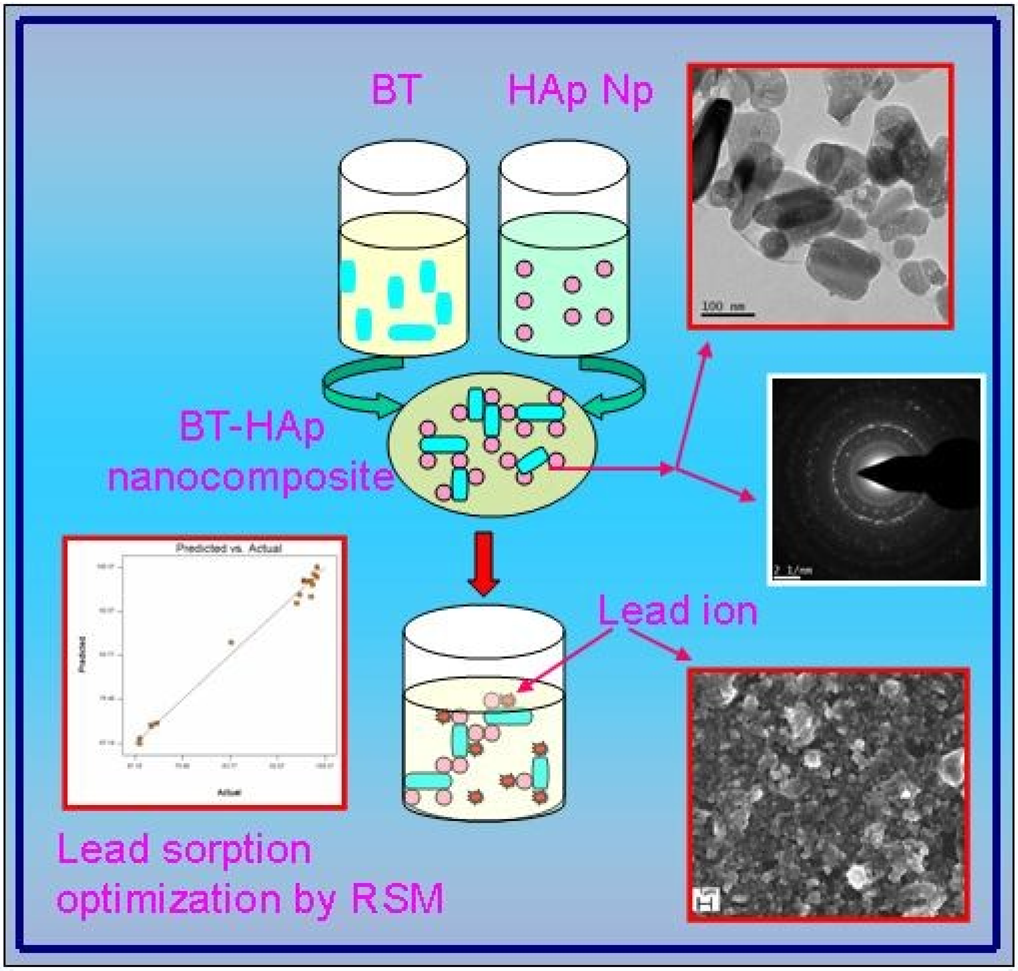

Fig. 1: Schematic of nanocomposite preparation process with changes in morphology

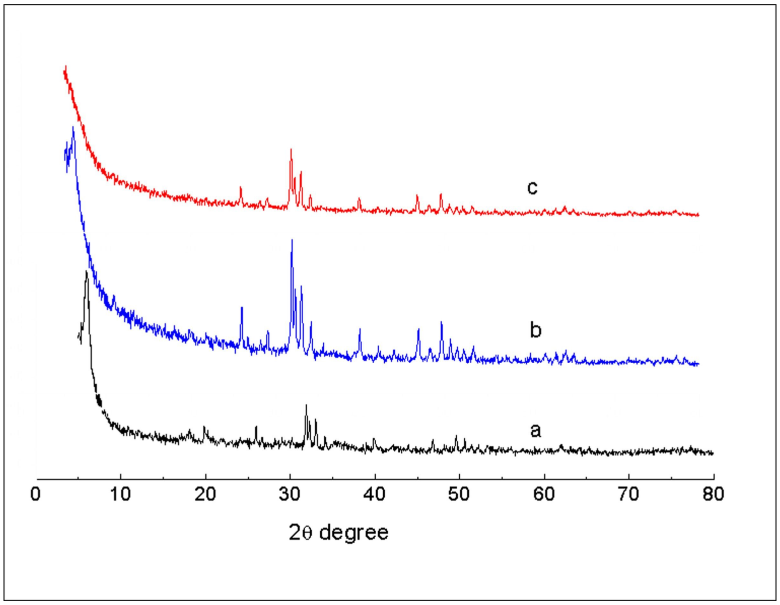

Fig. 2: XRD pattern of nanocomposite for: BT-HAp- (a) pH-3, (b) pH-7 and (c) pH-10

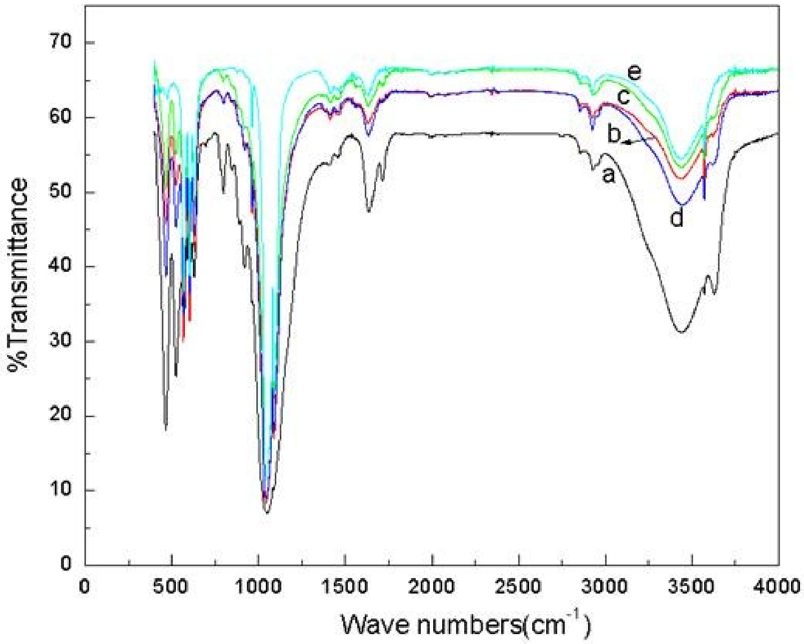

Fig. 3: FTIR spectra of the nanocomposite for: (a) pH-3, (b) pH-7, (c) pH-10, (d) after sorption and (e) HAp Np.

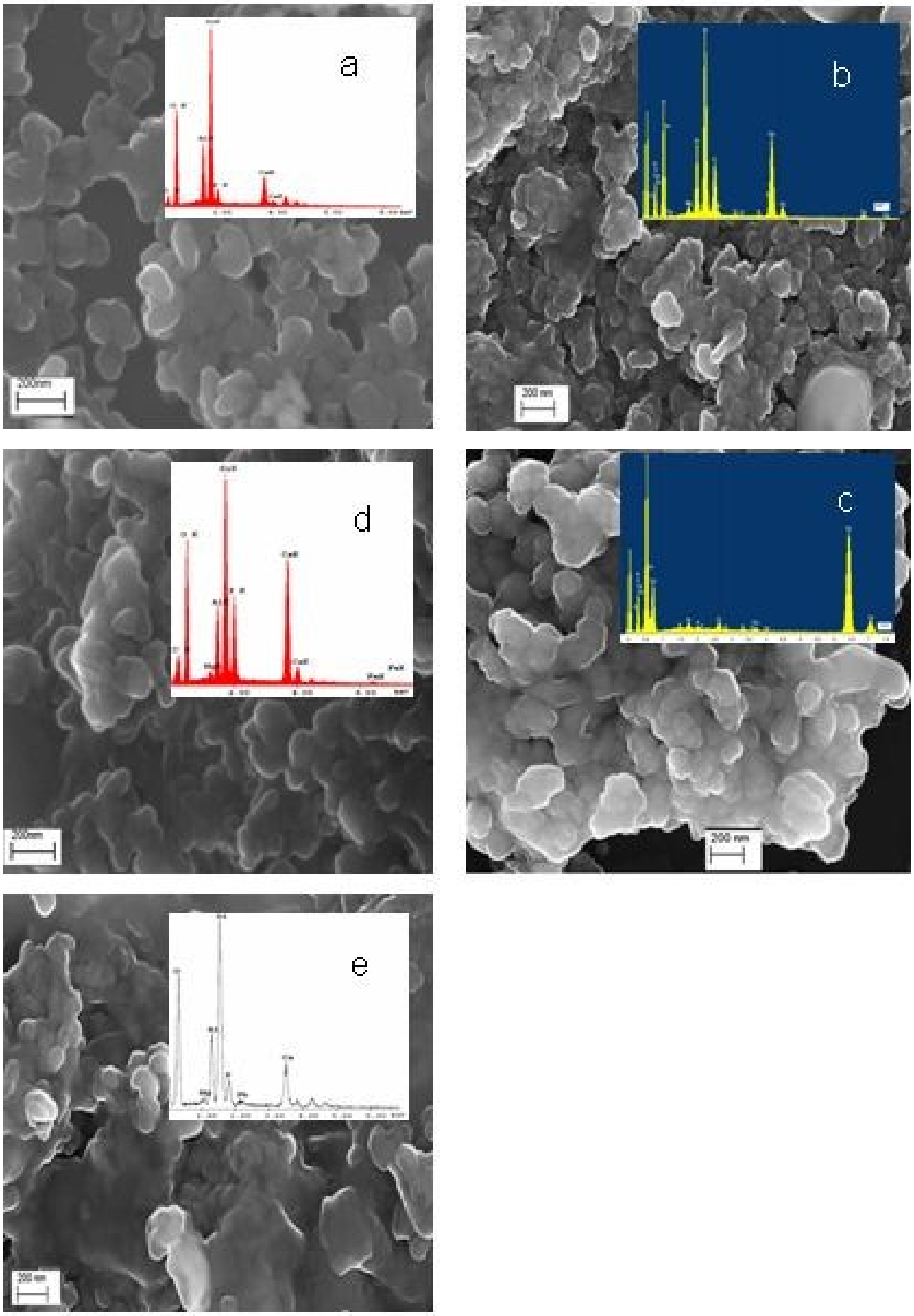

Fig. 4: FESEM and EDX spectra: (a) HAp nanoparticles, nanocomposites: (b) BT-HAp-3, (c) BT-HAp-7, (d) BT-HAp-10 and (e) after sorption process

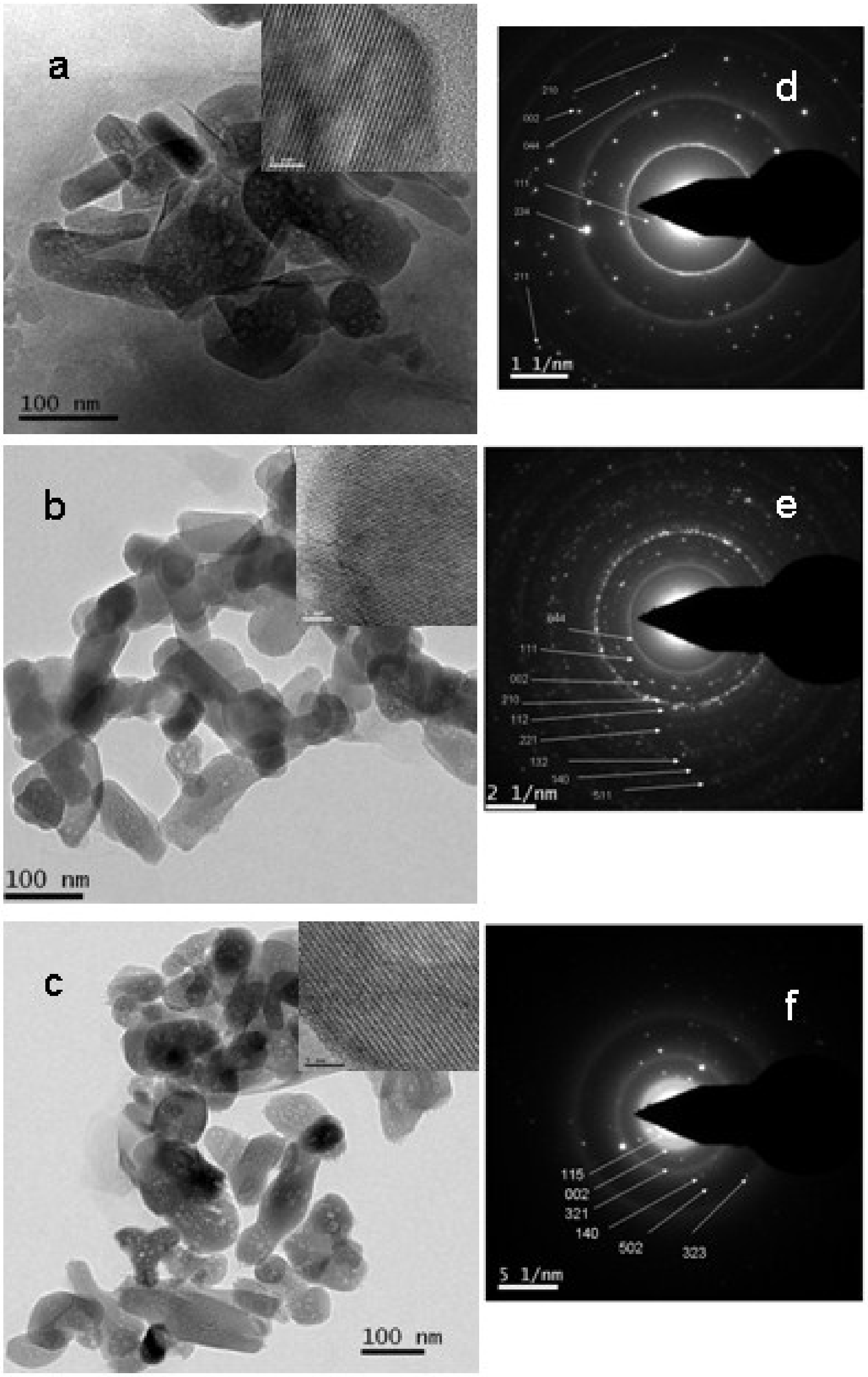

Fig. 5: TEM image of BT-HAp nanocomposite: Bright field images (a-c) with HRTEM in inset and (d-f) SAED pattern

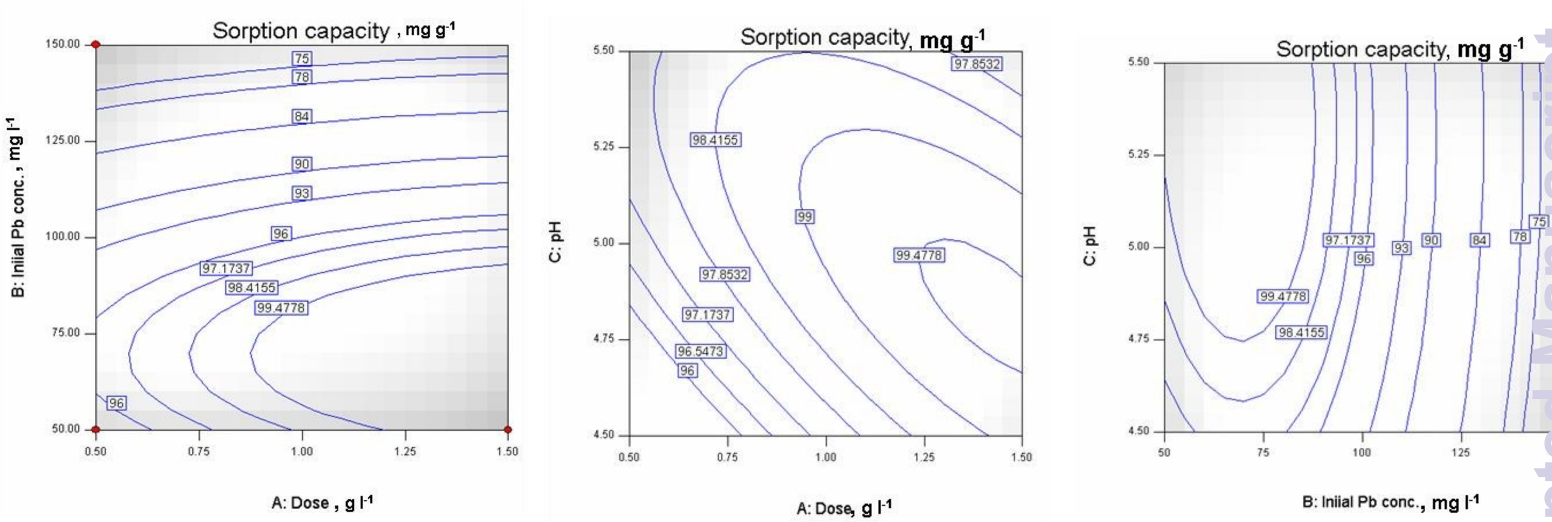

Fig. 6: Contour plots demonstrating the effect of independent variable on sorption capacity. (a) dose vs. Initial Pb conc., (b) dose vs. pH and (c) initial Pb conc. Vs. pH.

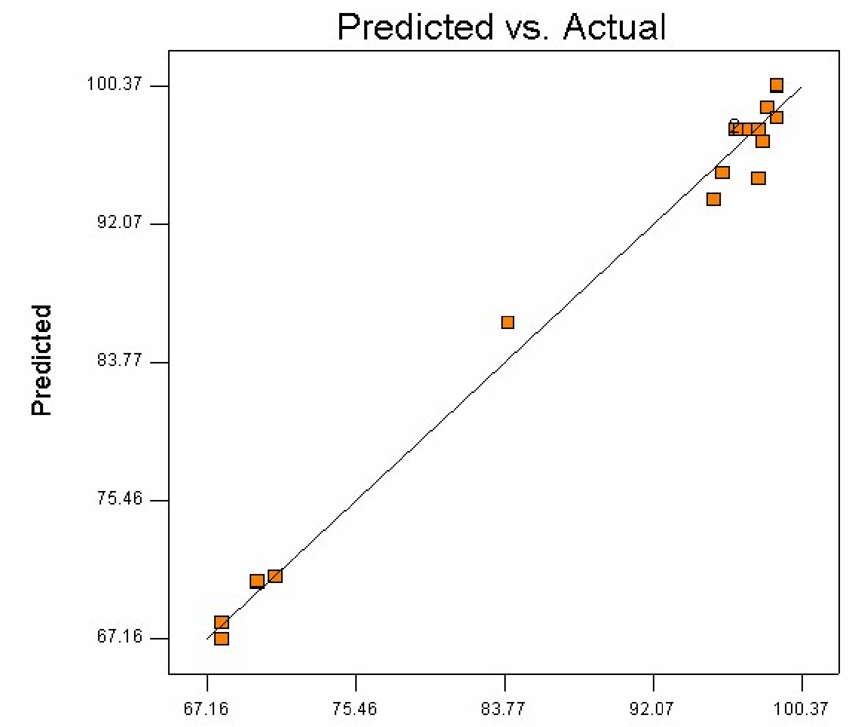

Fig. 7: Validity of model: Actual vs. Predicted plot